Selective targeting of non-centrosomal AURKA functions through use of a novel targeted protein degradation tool

Richard Wang[1], Ahmed Abdelbaki[1], Camilla Ascanelli[1], Alex Fung[1,3], Tim Rasmusson[2,4], Karen Roberts[2] and Catherine Lindon[1*]

[1] Department of Pharmacology, University of Cambridge, Tennis Court Road, CB2 1PD, UK

[2] Discovery Sciences, R&D, AstraZeneca, Cambridge, CB4 0WG, UK

[3] Current address: University of Cambridge School of Clinical Medicine, Addenbrooke's Hospital, Hills Road, Cambridge, CB2 0SP

[4] Current address: Bristol Myers Squibb, Cambridge, MA 02140, USA

Abstract

Targeted protein degradation tools are becoming a new therapeutic modality, allowing small molecule ligands to be reformulated as heterobifunctional molecules (referred to as 'PROTACs', for PROteolysis Targeting Chimeras) that recruit a ubiquitin ligase to the target of interest, leading to ubiquitination of the target and its destruction via the ubiquitin-proteasome system. A number of PROTACs against targets of clinical interest have been described, but detailed descriptions of the cell biology modulated by PROTACs are missing from the literature. Here we describe the functional characterization of a PROTAC derived from AURKA inhibitor MLN8237 (alisertib). We demonstrate efficient and specific destruction of both endogenous and overexpressed AURKA by Cereblon-directed PROTACs. At the subcellular level, we find differential targeting of AURKA on the mitotic spindle compared to centrosomes. The phenotypic consequences of PROTAC treatment are therefore distinct from those mediated by alisertib, and in mitotic cells differentially regulate the centrosome- and chromatin- based microtubule spindle assembly pathways. In interphase cells we find that PROTAC-mediated clearance of non-centrosomal AURKA, and not PROTAC-mediated inhibition of its activity, efficiently modulates the cytoplasmic role played by AURKA in mitochondrial dynamics, whilst the centrosomal pool is refractory to PROTAC-mediated clearance. Our results point to differential accessibility of subcellular pools of substrate, governed by substrate conformation or localization in compartments more or less accessible to PROTAC action, a phenomenon not previously described for this new class of drugs.

Introduction

The advent of targeted protein degradation tools that exploit the endogenous protein degradation machinery to eliminate disease proteins from the cell has started a revolution in therapeutic strategy and drug design[1]. One novel way to target proteins for degradation is through PROteolysis Targeting Chimeras (PROTACs), consisting of a chimeric molecule that binds at one end to a protein target, and at the other to a ubiquitin ligase (E3), most commonly the Cereblon (CRBN) substrate recognition protein together with the CUL4A E3 ligase complex, or to the von Hippel Lindau (VHL) protein in association with the CUL2 complex[2,3]. This PROTAC-mediated ternary complex formation between functional E3 and target protein facilitates ubiquitin transfer[4], leading to ubiquitination of the target and its proteolysis at the 26S proteasome.

This new paradigm of 'event-driven' pharmacology (in contrast to the use of traditional 'occupancy-based' drugs) holds great hope for the development of catalytic drugs able to work at lower doses and with higher specificity than the ligands from which they are derived. Moreover, the altered pharmacodynamics of substrate destruction versus inhibition raises the possibility of repurposing small molecule ligands (including those that have failed clinical trials as inhibitors of their targets) into PROTACs. However, although a number of publications document the success of novel PROTACs in eliminating their cellular targets, there has been little impact of this technology so far in the field of cell biology. PROTACs have clear potential as a method for investigating cellular protein functions on a timescale more favourable than siRNA-mediated interference and in a way that does not depend on effective inhibition of an enzymatic function. In this study, we investigate the properties of a novel PROTAC tool based on a known small molecule inhibitor of the mitotic kinase Aurora A (AURKA), MLN8237 (also known as alisertib)[5–7].

AURKA is a well-studied regulator of mitosis, playing critical roles in centrosome maturation, mitotic timing, microtubule nucleation and spindle assembly[8,9]. Distinct populations of AURKA are either recruited to centrosomes by CEP192, or on spindle microtubules (MTs) via the MT-associated protein TPX2. These separate populations can be independently perturbed through disruption of either interaction[10–12]. AURKA activity at centrosomes contributes to mitotic entry. Activation of AURKA is thought to occur either through auto-phosphorylation in the T-loop (at T287/288), a process promoted by CEP192 oligomerization at the centrosomes, or through interaction with a number of known binding partners that act to stabilize the 'DFG-In" conformation to favour kinase activity independently of T-loop phosphorylation[13–15]. The best-known of these interactors is TPX2. At nuclear envelope breakdown (NEB), TPX2 is released by importin-α, under the influence of the RanGTP gradient around the mitotic chromosomes, to bind and activate AURKA. *In vitro* tests show that binding by TPX2 and T-loop phosphorylation independently activate AURKA approximately 100-fold[16,17]. These separable intracellular AURKA activities (defined by pT288 at the centrosomes and TPX2 binding around chromatin) contribute to distinct pathways of MT nucleation that act together to achieve mitotic spindle assembly. Critical targets of AURKA in both pathways are NEDD1 and TACC3. Recruitment and phosphorylation of NEDD1 allows recruitment of the γ-TURC nucleating complex whilst phosphorylation of TACC3 promotes assembly of a pTACC3-AURKA-clathrin complex proposed to stabilize parallel MTs in the spindle.

AURKA undergoes targeted proteolysis in every cell cycle as a substrate of the Anaphase-Promoting Complex (APC/C) ubiquitin ligase at mitotic exit[18,19]. However, AURKA is detectable in interphase cells and has been attributed a number of non-mitotic roles including ciliation control, cell cycle regulation of MYCN-dependent transcription, DNA damage pathways and mitochondrial regulation[20–23]. Overall, there is a growing interest in the roles played by AURKA outside of mitosis and their contribution to its cancer-promoting activity. AURKA has long been a postulated therapeutic target due to its well-documented overexpression in cancer, although the role it plays in oncogenesis is far from clear. Recent structural and conformational studies have led to improved understanding of its mode of activation and the realization that multiple active forms may persist through interphase that depend on different binding partners. Recent work from our lab has shown that un-degraded AURKA retains activity after mitosis[24].

Therefore, a PROTAC tool able to eliminate AURKA protein could be an important cell biology tool as well as a potential therapeutic strategy. Here we test characteristics of PROTAC activity directed against

AURKA and investigate the cell biology that accompanies targeted protein degradation of this critical cellular target.

Materials and Methods

Cell culture and synchronization

U2OS and HeLa cells were cultured in DMEM (Thermo Fisher Scientific) supplemented with 10% FBS, 200 µM Glutamax-1, 100 U/ml penicillin, 100 µg/ml streptomycin, and 250 ng/ml fungizone at 37°C with 5% CO_2. hTERT-RPE-1 cells were cultured in DMEM:F12 mix with the same supplements. RPE-1 AURKA^{KI} cells and RPE-1 AURKA^{TO} cells additionally with 500 µg/ml geneticin.

For assaying live cell degradation of AURKA-Venus^{KI} and AURKA-Venus^{TO} in mitotic arrested cells, 1.5 x 10^4 RPE1 AURKA-Venus^{KI} cells were seeded per well in 8-well slides (Ibidi GmbH) and treated for 16 hr with 10 µM S-trityl L-cysteine (STLC) (Tocris Bioscience) prior to PROTAC treatment.

For assaying live cell degradation of AURKA-Venus^{TO} in G_2 arrested cells, 1.5 x 10^4 RPE1 AURKA^{TO} cells were seeded per well in 8-well slides (Ibidi GmbH) and treated for 16 hr with 10 µM RO3306 (Tocris Bioscience) prior to PROTAC treatment.

For assaying degradation by immunoblot of cell extracts, 2 x 10^5 AURKA-Venus^{KI} cells were seeded in 6-well plates prior to 16 hr STLC treatment and addition of test compounds.

Cells for immunofluorescence were seeded on glass coverslips and enriched for the population of mitotic cells by release from a single 24 hr block with 2.5 mM Thymidine. Cells were fixed 10 hr after release, to include the time of treatment with test compounds.

For assaying mitochondrial fragmentation, U2OS FZR1^{KO} cells seeded on 8-well Ibidi slides were incubated for 15 minutes at 37ºC in MitoTracker Red® CMXRos(Thermo Fisher Scientific) as per manufacturer's instructions.

Drug treatments

AURKA PROTACs ≤ 1 µM, Pomalidomide (synthesised in-house)
Aurora A kinase inhibitor MLN8237 ≤ 1uM (Stratech, Ely, UK)
MG132 42 µM (Alfa Aesar)
RO3306 10 µM (Tocris Bioscience)
APCin 20 µM (Bio Techne)
ProTame 40 µM (R&D Systems)

Cell transfection

Cells were transfected with 1µg of plasmids using electroporation with Neon Transfection System (Thermo Fisher Scientific) using the following parameters: pulse voltage 150 V, pulse width 10 ms, and 2 pulses total on the transfection device according to the manufacturer's protocol. AURKA and AURKB plasmids used were expressed with C-terminal Venus tags in pVenus-N1 vector. Δ32-66, S51D, S155R and Δ67 versions of AURKA were generated by PCR mutagenesis, with cloning maps available on request.

CEP192 knockdown was achieved by electroporating the oligo duplex: 5'-GGAAGACAUUUUCAUCUCUtt-3' and 5'-AGAGAUGAAAAUGUCUUCCtt-3' (Sigma).

Immunoblotting

Cell extracts were prepared in NuPage (Invitrogen) SDS sample buffer with 100 µM DTT, Extracts were syringed and boiled prior to electrophoresis on NuPage precast 4-12% Bis-Tris SDS-PAGE gels (90 min, 150 V, 80 W). Proteins were transferred on to Immobilon-FL PVDF (Sigma) membrane using a wet transfer XCell IITM Blot Module system (120 mins, 30 V, 80 W). Blocking and incubations were performed in phosphate-buffered saline (PBS), 0.1% Tween-20, 5% low-fat milk (TBST and 3% BSA for phosphoantibodies) either overnight at 4 °C or for 1 hour at room temperature. Signals were quantified by enhanced chemiluminescence detection, or using fluorophore-conjugated secondary antibodies, scanned on an Odyssey® Imaging System (LI-COR Biosciences).

Primary antibodies for immunoblot were as follows: AURKA mouse mAb (1:1000; Clone 4/IAK1, BD Transduction Laboratories), phospho-Aurora A (Thr288)/Aurora B (Thr232)/Aurora C (1:1000; clone D13A11 XP® Rabbit mAb, Cell Signalling), rabbit polyclonal TPX2 antibody (1:1000; Novus Biological), AURKB rabbit polyclonal antibody (1:1000; Abcam ab2254), mouse mAb Cyclin B1 (1:1000; BD 554177), rabbit polyclonal beta-tubulin (1:2000; Abcam ab6046), GAPDH rabbit mAb (1:400; Cell Signaling Technology #2118), TACC3 rabbit polyclonal antibody (1:1000; gift from F. Gergely), CEP192 affinity-purified rabbit polyclonal antibody (1:1000; Gift from L. Pelletier[25]).

Secondary antibodies used were Polyclonal Goat Anti-Rabbit or Polyclonal Rabbit Anti-Mouse (1:1000) HRP-conjugated (Dako Agilent), or IRDye® 680RD (1:20,000)- or 800CW (1:10,000)-conjugated for quantitative fluorescence measurements on an Odyssey® Fc Dual-Mode Imaging System (LICOR Biosciences). IRDye® conjugated antibodies were prepared in PBS, 0.1% Tween-20, 5% FBS, 0.01% SDS.

Immunofluorescence

Cells were seeded at 2 x 10^4 onto glass coverslips and then fixed with cold 100% methanol (−20°C), permeabilized and blocked with 3% bovine serum albumin (BSA) and 0.1% Triton X-100 in PBS (blocking buffer) for 15 min at room temperature. Cells were washed 3 times in PBS with 0.1% Triton X-100 for 5 min each prior to 1 hour incubation with primary antibodies diluted in blocking buffer at room temperature in a humidity chamber. Slides were then washed 3 times again in PBS with 0.1% Triton X-100 for 5 min each before incubation with secondary antibodies diluted in blocking buffer for 45 min at room temperature in a humidity chamber. DNA was stained with Hoechst-33342 (1µg/mL) and coverslips were mounted with Prolong Gold antifade reagent.

Primary antibodies used for immunofluorescence were as follows: AURKA mouse mAb. (1:1000; Clone 4/IAK1, BD Transduction Laboratories), AURKA rabbit polyclonal (1:1000; Abcam ab1287), PLATS2 mouse mAb (1:1000; Clone. ST-3B11, Caltag Medsystems), TACC3 rabbit polyclonal antibody (1:1000; gift from F. Gergely), TPX2 rabbit polyclonal (1:1000; Novus Biological)

CEP192 affinity-purified rabbit polyclonal antibody (1:1000; Gift from L. Pelletier), beta-tubulin rabbit polyclonal (1:1000; Abcam ab6046), beta -tubulin mouse mAb (1:300; Sigma T4026)

Secondary antibodies used were: Alexa Fluor 488 anti-mouse and Alexa Fluor 568 anti-rabbit (Thermo Fisher Scientific).

Microscopy

All images were acquired on automated epifluorescence imaging platforms based on Olympus IX81 or IX83 inverted microscopes (Olympus Life Science, Southend-on-Sea, UK) with LED illumination source and motorized stage. Time-lapse was carried out using cells seeded on Ibidi 8-well slides, and imaged at 37°C in L-15 medium/ 10% FBS using a 40X NA1.3 OIL objective. Epifluorescent stacks of fixed cells after processing by IF were acquired using 60X NA 1.0 OIL objective with 200 nm step. Image acquisition was controlled by Micro-Manager[26] and images exported as tiff files.

Image analysis, quantifications and statistical analyses

Images were analysed using FIJI[27], measuring net green intensity (T_i) of cell after background subtraction at T0 and T200 mins. Picked cells which remained in prometaphase for the duration of the 200 mins. % degradation measured as ($T0_I$ – $T200_I$)/ $T0_I$.

Linescans were carried out using the BAR package in FIJI.

Mitochondrial lengths were analysed using MicroP[28].

Quantified data analyses were plotted using GraphPad 6.01 (San Diego, CA, USA). Results were analyzed with ANOVA, Student's *t*-test or Mann Whitney U test (non-parametric) as indicated in figure legends. Significant results are indicated as $p < 0.05$ (*), $p \leq 0.01$ (**), $p \leq 0.001$(***), $p \leq 0.0001$ (****). Values are stated as the mean ± SDs.

AURKA and AURKB biochemical assays

AURKA and AURKB biochemical assays were performed as part of the ThermoFisher SelectScreen kinase profiling service. These assays were in the Z'-Lyte activity format and used full-length purified protein and ATP at K_m (10 μM for AURKA, 75 μM for AURKB).

Results

We set out to investigate the action of AURKA-directed targeted protein degradation tools (PROTACs) against AURKA in single cell time-lapse assays using cell lines that we have previously described[29]: an AURKA-Venus knock-in line in RPE1 cells (AURKA-Venus^{KI}) where AURKA-Venus recapitulates expression of the endogenous protein (undetectable in interphase cells and strongly upregulated for mitosis), and a line expressing exogenous AURKA-Venus under tetracycline control (RPE1FRT/TO-AURKA-Venus, AURKA-Venus^{TO}) where higher levels of expression occur throughout the cell cycle. We used AURKA-Venus^{KI} and AURKA-Venus^{TO} cells arrested in mitosis by an agonist of the Spindle Assembly Checkpoint (SAC), STLC, to test the activity of PROTAC compounds that link the well characterized inhibitor of AURKA MLN8237 to small molecule ligands for CRBN and VHL (Table 1, Figure 1).

We synthesised eight PROTAC molecules consisting of the well-characterised inhibitor of AURKA, MLN8237, linked to either a known ligand of von Hippel-Lindau (VHL) E3 ligase[30] or to the thalidomide derivative, pomalidomide, to recruit Cereblon (CRBN) E3 ligase[31]. As the linker is an integral part of the PROTAC molecule and linker length can be a key determinant of PROTAC function[32], we designed four molecules for each of the MLN8237-CRBN or -VHL combinations with varying polyethylene glycol (PEG) linker lengths.

We found that CRBN-based PROTAC compounds were able to elicit destruction of both AURKA-Venus^{KI} and AURKA-Venus^{TO} in time-lapse movies of mitotic arrested cells (Figure 1A-D). Compound D, a Cereblon driven PROTAC, reduced AURKA levels in a dose dependent manner (Figure 1B, C), with an EC_{50} in the 100 nM range (Figure 1B). At a dose of 1μM, Compound D caused loss of AURKA-Venus with $t_{1/2}$ approximately 2 hours (Figure 1C). The activity of the PROTAC against AURKA-Venus^{KI} in time-lapse assays (Figure 1D), or against endogenous AURKA in extracts from mitotic arrested HeLa cells (Figure 1E, F), appeared to correlate with linker length, suggesting that topological constraints limit the efficacy of PROTAC action. The VHL-based PROTACs tested were inactive in all but one dose (Figure 1D). Taken together, the most efficient PROTAC tested in these initial experiments was Compound D, which we named AURKA-PROTAC-D (PROTAC-D). We tested the correlation between linker length and efficacy of the PROTAC by creating a new compound with extra-long linker, Compound DX (Table 1). As predicted, Compound DX reduced AURKA levels more efficiently than PROTAC-D (Figure 1G). We tested the specificity of PROTAC action of CRBN-directed compounds in further experiments (Figure 1H, I) demonstrating that neither MLN8237 nor the CRBN ligand (pomalidomide) on its own affected AURKA levels (Figure 1H). In addition, the action of Compound D was blocked by competition with excess pomalidomide (Figure 1I), supporting that recruitment of Cereblon E3 holo-complex was necessary for AURKA level reduction.

While analysing these experiments, we noticed that AURKA-Venus^{KI} cells arrested in mitosis with STLC were more likely to exit mitosis after treatment with PROTAC than after treatment with DMSO. As we wanted to be able to separate PROTAC treatment effects caused by target degradation from any residual inhibitory effects caused by just on-target or off-target engagement, we used Compound A (Cpd A) as a negative control in this and subsequent experiments. Cpd A is a MLN8237-VHL molecule with linker length consistent with PROTAC-D that showed no PROTAC activity against AURKA (Figure 1D). Cpd A had a small and non-significant effect in promoting mitotic slippage (consistent with a weak inhibition of AURKA activity) compared to PROTAC-D (Figure 2A). Since AURKA is itself a substrate of mitotic exit degradation under control of the APC/C^{FZR1} [33], failure of the SAC, leading to activation of the APC/C, would be predicted to result in degradation of AURKA independently of PROTAC-mediated ubiquitination. Therefore, in the single cell mitotic degradation assays shown in Figure 1, we quantified only cells that remained arrested in mitosis for the duration of the assay. However, we also carried out experiments to test directly whether mitotic degradation pathways were involved in PROTAC-D-driven disappearance of AURKA-Venus, using a combination of drugs (APCin, proTAME) that inhibits the activity of the APC/C ubiquitin ligase[34]. Degradation of AURKA-Venus in response to PROTAC-D was not prevented by inhibition of APC/C (Figure 2B, C) and was therefore independent of mitotic exit.

The effect of PROTAC-D in promoting mitotic exit could potentially be explained by a number of studies showing a role for AURKA in the SAC[35–37], but could also occur through 'mitotic slippage', should there be any non-specific targeting of Cyclin B1 by PROTAC-D in the presence of an active SAC[38]. We tested this possibility using a RPE1-cyclin B1-Venus^{KI} line[39]. Degradation of Cyclin B1-Venus and escape of cells from SAC-induced arrest were both strongly promoted by PROTAC-D (Figure 2D, E), and weakly by Cpd A. However, in contrast to AURKA-Venus^{KI} degradation (Figure 2B), Cyclin B1-Venus^{KI} degradation measured upon PROTAC-D treatment was sensitive to APC/C inhibition (Figure 2F). These results allowed us to

conclude that Cyclin B1-Venus degradation in the presence of PROTAC-D is the result of weakened SAC and that Cyclin B1 is not targeted directly by PROTAC-D.

In further experiments to test that degradation of AURKA in response to PROTAC-D was independent of the well-characterized APC/C-dependent pathway, we used versions of AURKA known to be resistant to APC/C-mediated degradation. AURKA possesses an atypical APC/C degron motif, the so-called A-box, in its N-terminal disordered region[40]. The A-box function appears to be negatively regulated through phosphorylation on Ser51, since phospho-mimic substitution at this site blocks mitotic degradation of AURKA[33,41,42]. We found, using single cell time-lapse degradation assays, that an A-box deleted (Δ32-66) version of AURKA-Venus stably expressed in an RPE-FRT/TO line was efficiently degraded in response to PROTAC-D (Figure 2G). We concluded that PROTAC-mediated degradation of AURKA does not require the substrate motif essential for its canonical degradation, either for ubiquitination, or at any downstream step in substrate processing at the 26S proteasome. We additionally tested the S51D version of AURKA-Venus alongside the WT protein in time-lapse degradation assays, after transient electroporation into U2OS cells. We found not only that both WT and 'non-degradable' S51D were sensitive to PROTAC-D in mitotic cells (Figure 2H), but that they were also sensitive in interphase cells (Figure 2I), as further confirmation that PROTAC-mediated processing of AURKA for destruction is independent of cell cycle-dependent pathways. We note that the measured rate of degradation is lower in interphase cells than mitotic cells, most likely because degradation is masked by ongoing synthesis (observed as accumulation of the protein in DMSO-treated control cells). We concluded that degradation of AURKA measured in response to PROTAC-D treatment is a direct consequence of PROTAC-D-mediated targeting. Furthermore, since some experiments were carried out using high-level transient expression of electroporated constructs (Figure 2H, I), PROTAC-D appears potent enough to clear target protein at significant levels of overexpression in the cell.

Next, we asked whether target destruction mediated by PROTAC-D was specific for AURKA. Since the PROTAC target ligand MLN8237 has a degree of selectivity for AURKA over its cellular paralogue AURKB, but is not completely specific (it inhibits AURKB activity at doses of ≥ 50 nM[5], and the reported selectivity ratio AURKA-TPX2$_{(1-43)}$: AURKB-INCENP$_{(783-918)}$ is approximately 5-fold[6]), we might expect to find some degradation of AURKB in response to a PROTAC carrying the MLN8237 warhead. Furthermore, considering that within the mitotic cell AURKA resides in multi-protein complexes governing its localization and function, we hypothesized that the 'ectopic' recruitment of ubiquitination machinery by PROTAC-D might lead to ubiquitination and destruction of AURKA binding partners. Therefore, we examined if PROTAC-D caused reduction in cellular levels of AURKB, or of two well-known interacting partners of AURKA, TPX2 and TACC3 (Figure 3).

Surprisingly, we found that treatment with PROTAC-D caused very little degradation of AURKB-Venus in an inducible U2OS cell line[43] (Figure 3A), or of endogenous AURKB in HeLa cells (Figure 3B, C). We also found no degradation of endogenous TPX2 in mitotically-enriched HeLa cells after 3 hours of treatment with PROTAC-D (Figure 3B, C). TPX2 and TACC3 levels were unchanged in cells treated for up to 12 hr, when endogenous AURKA was no longer detectable (Figure 3D). Therefore PROTAC-D-mediated destruction is highly specific for AURKA. The resistance of AURKA binding partners to PROTAC-D

treatment suggests that the ubiquitination step is highly specific for the AURKA moiety of mitotic complexes, or alternatively, that only unbound AURKA is targetable by PROTAC-D.

Given the unexpected resistance of AURKB to AURKA PROTAC action, we compared *in vitro* kinase inhibition activities for AURKA and AURKB of PROTACs –D and –DX, Cpd A, and their warhead MLN8237. We found that both of the PROTACs had greater selectivity for AURKA over AURKB than MLN8237 in kinase inhibition assays (fold selectivity of PROTAC-D = 21.6, PROTAC-DX = 23.7, MLN8237 = 8.3) (Figure 3E), explaining the lack of AURKB degradation seen in Figures 3A-C). The increased selectivity for AURKA suggests that the increased size and/or complexity of the PROTAC creates new steric parameters influencing target discrimination, and is consistent with published findings from others that the requirement for ternary complex formation in PROTAC action can build a further layer of specificity into drug action[44,45]. Comparing IC_{50} values for inhibition of *in vitro* kinase activity of PROTAC-D and -DX versus MLN8237, we found that inhibition of AURKA kinase activity by the PROTAC molecules is weaker than that mediated by MLN8237 (5-10 fold). Interestingly PROTAC-DX, which has stronger PROTAC activity in comparison to PROTAC-D (Figure 1G), does not have higher activity in this assay (Figure 3E). This finding is in line with the idea that the efficiency of PROTAC activity is not only impacted by binding affinity to the target or E3 ligase, but also related to efficiency of ternary complex formation between E3 and target protein[46].

Having validated PROTAC-D as an effective and specific tool for depletion of cellular AURKA, we investigated how PROTAC-mediated AURKA destruction would compare to enzymatic inhibition as a method for down-regulating AURKA functions in mitotic cells. We fixed cell populations synchronized for passage through mitosis and treated for 4 hr with parallel doses of PROTAC-D or MLN8237, or with DMSO as a negative control, and stained them by immunofluorescence (IF) for the presence of AURKA, markers of AURKA activity and tubulin, in order to assess the phenotypic consequences of drug treatment (Figure 4). We looked first at AURKA staining and found that cells treated with PROTAC-D displayed a marked loss of the pool of AURKA associated with the spindle (seen in DMSO-treated controls). However, AURKA was preserved at the centrosomes (Figure 4A). By contrast, treatment with MLN8237 abrogated almost all AURKA localization to centrosomes, consistent with the known role of AURKA activity in centrosome maturation that includes recruitment of AURKA to the pericentriolar material (PCM)[47]. This finding suggested that the centrosome-associated pool of AURKA seen in PROTAC-D-treated mitotic cells would be unexpectedly fully active (that is, neither degraded nor inhibited by PROTAC treatment). We tested this idea by measuring levels of pSer83-LATS2 as a well-known centrosomal marker of AURKA activity, finding that this marker was entirely resistant to PROTAC-D treatment (at doses sufficient to deplete most of the cellular pool of AURKA), whilst responding in dose-dependent fashion to MLN8237 (Figure 4B,C).

Given the >5-fold difference in enzyme inhibition of PROTAC-D and MLN8237 (Figure 3E) and the likelihood that the intracellular dose of PROTAC-D is limited by its size[48], we examined the phenotypic consequences of treatment over a 10-fold range of doses of both drugs, scoring mitotic figures according to the categories illustrated in Supplementary Figure S1. Dose-response to MLN8237 treatment is characterized by progression from spindle orientation defects at low doses to spindle assembly defects (multipolar spindles, 'small' spindles) at intermediate doses, to lack of MT nucleation at a dose of 250 nM (Figure 4D and as previously described[5]). We were surprised to find that PROTAC-D-treated cells showed none of these defects (Figure 4D, E). Even at the highest dose tested (250 nM), we did not see the

orientation defects characteristic of low dose inhibition of AURKA activity[5,49]. Instead, we observed that the mitotic spindles were shorter in length after PROTAC treatment. Distribution of the centrosomal pLATS2 staining shown in Figure 4B confirms that the pole-to-pole distance of correctly oriented bipolar spindles is reduced (Figure 4F).

Our finding of 'short spindles' was reminiscent of the previously reported finding that specific perturbation of AURKA binding to TPX2 controls spindle length independently of any effect on assembly[10] which can occur under the influence of the centrosomal AURKA pool. Therefore, we hypothesized that PROTAC-D had selectively depleted the TPX2-associated pool of AURKA to eliminate the chromosome-centred MT nucleation pathway whilst leaving the centrosomal pathway untouched. We decided to test this idea using a modified cell synchronisation assay that would better allow us to compare the roles of kinase inhibition and target degradation in mitotic cells independent of their different effects on AURKA-dependent centrosome maturation. We pre-synchronised cells at metaphase by release of cells arrested for 24 hours in Thymidine into APCin/proTAME for 6 hours. We then treated metaphase-arrested cells with different doses of MLN8237, PROTAC-D and Cpd A for 3 hours before fixing them for IF analysis. We reasoned that use of these drugs would reveal phenotypes resulting from degradation of AURKA, distinguishing them from those arising purely out of kinase inhibition: Degradation-dependent effects would be sensitive to PROTAC-D whilst insensitive to Cpd A treatment (with sensitivity to MLN8237 depending on kinase-dependence of the phenotype studied); kinase inhibition phenotypes would show greatest sensitivity to MLN8237, whilst PROTAC-D and Cpd A would show weak or no effect, but importantly, they would produce the same effect.

Following fixation, we stained cells for AURKA and its interactors CEP192 and TPX2 (Figure 5). Similar levels of CEP192 at centrosomes after the different treatments confirmed that centrosome maturation had occurred in a large fraction of the cellular pool of metaphase cells (Figure 5A). Quantification of AURKA levels in these cells showed the total cellular pool of AURKA reduced more than three-fold after PROTAC-D treatment (Figure 5B). Measured AURKA levels were also somewhat lower (by about 30%) after treatment with Cpd A or with low (25 nM) or high (250 nM) doses of MLN8237. Since we have found that these treatments do not affect endogenous AURKA levels, nor AURKA-Venus levels in intact cells, we assumed that the reduced AURKA levels seen in IF reflected loss of AURKA in the fixation step, that could be a consequence of reduced interaction with the mitotic spindle. Indeed, MLN8237 and TPX2 may compete with each other for AURKA binding[50] (see Discussion). We measured pole-pole distances in this experiment and found them reduced by PROTAC-D treatment. AURKA inhibition with 25 nM MLN8237 also gave rise to short spindles, whereas Cpd A had no effect on spindle length (Figure 5C). We concluded that Cpd A and PROTAC-D both bind too weakly to AURKA to significantly inhibit its activity, and that the short spindle phenotype seen after PROTAC-D treatment depends on destruction of AURKA by PROTAC-D. Consistent with this conclusion, we observed that PROTAC-D alone of the drug treatments removed both cytoplasmic and spindle pools of AURKA (Figure 5D). Kinase inhibition mediated by 25 nM MLN8237 or 250 nM Cpd A caused some loss of signal from the spindle, but also increased cytoplasmic levels of AURKA (Figure 5D, E). Comparison of AURKA pixel intensities in fixed areas on the centrosome or neighbouring spindle confirmed that depletion of the spindle signal was greater than at the centrosome (Figure 5F). We concluded from our data that PROTAC-D preferentially targets the pool of AURKA that associates with TPX2 to govern mitotic spindle length. Moreover, because kinase inhibition assays indicate

that Cpd A and PROTAC-D bind AURKA with equivalent affinity (Figure 3E), we concluded that the short spindle phenotype seen after PROTAC-D - but not Cpd A - treatment (Figure 5C) depends on destruction of AURKA protein.

We investigated further why PROTAC-D treatment led to selective depletion of the spindle-associated pool of AURKA. This could result from conformation-dependent targeting by the PROTAC, with the preferred target being either the TPX2-bound pool, or a free pool of AURKA (provided this turns over faster with the TPX2-bound pool than the centrosomal pool). Alternatively, the AURKA pool at the centrosomes might be 'protected' from PROTAC action (for example if either the PROTAC or CRBN E3 ligase were excluded from the PCM matrix). We investigated this question further by measuring the efficacy of PROTAC-D treatment in living cells under conditions where AURKA-Venus localization is perturbed.

We first compared the responses to PROTAC-D treatment of different versions of AURKA-Venus: AURKA-S155R, a version of AURKA showing strongly reduced interaction with TPX2[51], and two N-terminally truncated versions of AURKA (Δ67, Δ127) that show increased localization to the nucleus in RO3306-arrested interphase cells (Supplementary Figure S2). We found that S155R showed a similar pattern of targeting by PROTAC-D to the wild-type version, suggesting that interaction with TPX2 would not influence targeting. Moreover sensitivity to PROTAC-D of both WT and S155R versions of AURKA-Venus was highly variable in interphase cells, suggesting that factors other than TPX2 regulate the sensitivity of AURKA-Venus to PROTAC-D. By contrast, we observed that degradation of Δ67 was enhanced and less variable. Δ67 was also more strongly localized to the nucleus. When we measured the nuclear versus cytoplasmic degradation of wild-type protein, we found that nuclear AURKA-Venus was more efficiently depleted than the cytoplasmic pool upon PROTAC-D treatment (Supplementary Figure S3). The AURKAΔ127 version was also strongly nuclear (and absent from centrosomes), but appeared to be a hyper-stable version of the protein, showing a tendency to accumulate in cells over the time-course of the experiment in absence of PROTAC treatment, and low responsiveness to PROTAC (Supplementary Figure S3). From these data we concluded that nuclear localization appears to favour targeting of AURKA by PROTAC-D, but that the unstructured N-terminal domain, or the lysine residues within it, are required for turnover of AURKA (both for proteostasis in unperturbed cells as well as response to PROTAC-D).

Given this experimental limitation in using truncated versions of AURKA-Venus, we turned instead to an experiment designed to investigate how targeting of the wild-type protein is affected by its subcellular localization. Since we had found endogenous AURKA to be more strongly depleted at the spindle than on centrosomes, we treated RPE1-AURKA-Venus^{KI} cells with siRNA against CEP192 (CEP192i) to displace AURKA from the centrosomes[11]. This relocalization of AURKA is readily observed in cells arrested in G2 phase when AURKA-Venus^{KI} expression is high (Figure 6A-C). We tested AURKA-Venus degradation in response to PROTACs under these conditions, and measured slightly increased degradation of AURKA-Venus by immunoblot (Figure 6D, E). We then tested the effect of CEP192i on mitotic cells, when a much larger pool of AURKA is normally recruited to centrosomes. In STLC-arrested cells we found that AURKA-Venus^{KI} delocalized from centrosomes after CEP192i (Figure 6F, G) was more readily degraded in response to PROTAC-D (Figure 6H). We concluded that PROTAC-D is unable to bring about efficient degradation of centrosome-localized AURKA-Venus.

Given the differential targeting of AURKA pools by PROTACs –D and -DX, we tested whether PROTAC-DX could act to down-regulate the cytoplasmic pool of AURKA that regulates the mitochondrial network during interphase[20,52]. Our recent work has found that excess AURKA present in FZR1^{KO} cells fragments the mitochondrial network[24]. We treated FZR1^{KO} cells with PROTAC-DX and Cpd A and found that PROTAC-DX, but not Cpd A, rescues mitochondrial morphology (Figure 7). Therefore PROTAC-DX is able to prevent interphase activity of AURKA in a manner that depends on destruction of the protein, since Cpd A, which has similar activity as an inhibitor of AURKA but is unable to bring about its degradation, is unable to suppress AURKA activity at the same dose. We conclude that PROTAC-mediated clearance is more efficient than kinase inhibition in downregulating cytoplasmic AURKA activity.

Discussion

We have described a small molecule that acts as a specific degrader of AURKA to clear endogenous, exogenous GFP-tagged, or overexpressed protein from the cell. Amongst the molecules we tested, successful degraders were CRBN-specific. Although we have not formally excluded the possibilities that VHL is insufficiently active in U2OS cells to generate degradation-competent ubiquitin conjugates in response to CpdA, or that the four linker constructs we tested all occluded ternary complex formation between AURKA and VHL, our observation that the same four linker constructs were all able to support PROTAC activity directed to CRBN are in line with the published finding that protein-protein interaction surfaces of CRBN are more favourable to stable ternary complex formation than the equivalent surfaces of VHL[46].

We found that the activity of CRBN-directed molecules correlated with linker length but was independent of the affinity of the compound for its AURKA target. Therefore, it is likely that our longer linkers promote the assembly of productive ternary complexes by bringing together AURKA and CRBN in an orientation that allows the E3 complex to ubiquitinate AURKA at appropriate lysine residues. The physical properties of the linker are critical parameters in PROTAC activity, and further optimisation of PROTAC-DX could include different linker patterns to alter linker flexibility, as well as lengths.

Compounds showing PROTAC activity against AURKA were several-fold less potent than their MLN8237 warhead in inhibiting AURKA activity *in vitro*, consistent with reduced affinity for their target. Indeed, we found no evidence for direct inhibition of cellular AURKA functions by PROTAC-D (that is, all functions we examined were insensitive to the control compound, Cpd A, which shows equivalent activity against AURKA in kinase inhibition assays but has no PROTAC activity). Therefore we concluded that binding of PROTAC-D is weak enough, and/or the molecule present at sufficiently low intracellular levels, to achieve targeted degradation of AURKA in absence of any significant inhibition of AURKA kinase activity, and without exhibiting the hook effect characteristic of heterobifunctional ligands[53].

We observed that clearance of AURKA from the cell is less efficient than that mediated by its cognate E3, APC/C-FZR1 ($t_{1/2}$ ~ 100 min vs $t_{1/2}$ ~ 45 min[18]). We speculate that even with further optimization, it seems unlikely that any PROTAC would eliminate AURKA faster than its cognate pathway, since the rate-limiting step for degradation of many ubiquitinated substrates is not recruitment to the 26S proteasome, but determinants of processing that are partly substrate-specific (such as unfolding of substrate at the

proteasome) and partly determined by the configuration of ubiquitin chains[54]. Indeed, a recent study found that the presence of unstructured regions determines the PROTAC mediated degradation of VHL-directed substrates[55].

Interestingly, we tested versions of AURKA known to be resistant to APC/C-mediated degradation through mutation or removal of the essential N-terminal degron, and found them to be degraded in the presence of PROTAC-D as efficiently as wild-type AURKA. Therefore the position and topology of ubiquitin chains assembled on AURKA by CRBN and APC/C-FZR1 are likely to be very different.

We also observed that different cellular pools of AURKA substrate were differentially targeted by PROTAC treatment, since in mitotic cells the spindle-associated fraction of AURKA was eliminated whilst the centrosome fraction was preserved. Since the centrosomal pool of AURKA retained its activity, spindle assembly was buffered against the loss of the chromatin-associated TPX2-activated AURKA pool and the observed phenotype of PROTAC-D treatment in mitotic cells is therefore shortened spindles, consistent with a previous study of cells engineered to express a non-AURKA-binding version of TPX2[10]. Similarly, in interphase cells we observed that PROTAC-D treatment efficiently cleared the non-centrosomal pool of AURKA, but that centrosomal AURKA was preserved. Delocalization of the centrosomal pool through siRNA-mediated depletion of CEP192 promoted clearance of the total cellular pool of AURKA-Venus by PROTAC-D. Since centrosomal AURKA is efficiently inhibited by MLN8237, we would expect it to be accessible to bind MLN8237-derived PROTAC molecules. One explanation for its inaccessibility to PROTAC-D action could be that PROTAC-D at the centrosome fails to recruit CRBN or another component of the E3 complex required for ubiquitination of its target. Alternatively, there may be deubiquitinase enzymes active at the centrosomes that act to stabilize ubiquitinated AURKA.

Our results point to differential accessibility of subcellular pools of substrate, governed by substrate conformation or localization in compartments more or less accessible to PROTAC action, a phenomenon that has not previously been described for PROTAC agents acting via CRBN. Our finding of localized response to PROTAC-D is in contrast with treatment by the AURKA inhibitor alisertib, which promotes a clear dose-dependent depletion of pLATS2, a marker of AURKA activity at the centrosomes.

Given the complex conformational and spatial regulation of AURKA[15,17,56] we tested for conformation-specific targeting of the kinase using different versions of AURKA-Venus. The conformational dynamics of AURKA are strongly constrained through interaction with TPX2 [50,57,58], which favours the so-called 'DFG-In' active confirmation and it has been suggested that different functional pools possess distinct conformational properties that will modulate interactions with inhibitors[50]. In this study, alisertib/MLN8237 was shown to be a 'Type 1' inhibitor that promotes the inactive DFG-Out state, and TPX2 to oppose DFG-Out inducers, exhibiting negative cooperativity on binding with MLN8237[50]. In the DFG-Out state, the active site is more open (i.e. more accessible to MLN8237 or PROTAC-D). We expected therefore that a version of AURKA impaired in TPX2 binding (S155R[51]) should be more strongly degraded in response to PROTAC-D in presence of TPX2 (consistent with a model whereby PROTAC-D can more easily access AURKA in the DFG-Out conformation). However, we did not find a significant difference in response to PROTAC-D between S155R and wild-type AURKA. Instead, our data were consistent with the idea that the nuclear pool of AURKA is more efficiently degraded than the cytoplasmic pool. Further experiments are

required to establish whether these effects are related to the conformation of the target, or to the presence or activity of components of the UPS machinery engaged by PROTAC-D.

AURKA is of strong interest as a therapeutic target for various cancers, but despite extensive testing in clinical trials, alisertib has yet to reach the clinic. Our study is the first to describe a drug that shows specificity for different subcellular pools of AURKA, raising the possibility of developing PROTACs to fine-tune the activity of AURKA (and other targets that have shown disappointing clinical results) to produce cellular phenotypes that are potentially more desirable in pharmacological or therapeutic contexts. For example, alisertib-derived PROTACs could be used to target cytoplasmic functions of AURKA without inducing mitotic errors that are consequence of inhibiting AURKA function at the centrosome.

Acknowledgements

We thank Fanni Gergely and Laurent Pelletier for antibodies, Ian Storer, Iacovos Michaelides, Li Min and Yang Yue for Cpd D resynthesis and design and synthesis of Cpd DX. Andreas Hock made valuable comments on the manuscript. RKW was supported by BBSRC-DTP, AMA by a Yousef Jameel Scholarship from the Cambridge International Trust, and CA by a AstraZeneca-funded studentship. Work in CL's lab is funded by BBSRC (BB/R004137/1).

Author contributions

Study conceived and designed by CL and KR. TR synthesized compounds used. Experimental work was carried out and analysed by RKW, AMA, AF and CA. Manuscript written by CL and revised by KR, RKW, CA and AF.

References

1. Hanzl, A. & Winter, G. E. Targeted protein degradation: current and future challenges. *Current Opinion in Chemical Biology* **56**, 35–41 (2020).
2. Bondeson, D. P. *et al.* Catalytic in vivo protein knockdown by small-molecule PROTACs. *Nat. Chem. Biol.* **11**, 611–617 (2015).
3. Winter, G. E. *et al.* DRUG DEVELOPMENT. Phthalimide conjugation as a strategy for in vivo target protein degradation. *Science* **348**, 1376–81 (2015).
4. Lu, G. *et al.* UBE2G1 governs the destruction of cereblon neomorphic substrates. *Elife* **7**, (2018).
5. Asteriti, I. A. *et al.* The Aurora-A inhibitor MLN8237 affects multiple mitotic processes and induces dose-dependent mitotic abnormalities and aneuploidy. *Oncotarget* **5**, 6229–42 (2014).
6. de Groot, C. O. *et al.* A Cell Biologist's Field Guide to Aurora Kinase Inhibitors. *Front. Oncol.* **5**, (2015).
7. Manfredi, M. G. *et al.* Characterization of alisertib (MLN8237), an investigational small-molecule inhibitor of Aurora A kinase using novel in vivo pharmacodynamic assays. *Clin. Cancer Res.* **17**, 7614–7624 (2011).
8. Barr, A. R. & Gergely, F. Aurora-A: the maker and breaker of spindle poles. *J. Cell Sci.* **120**, 2987–2996 (2007).
9. Prosser, S. L. & Pelletier, L. Mitotic spindle assembly in animal cells: A fine balancing act. *Nature Reviews Molecular Cell Biology* **18**, 187–201 (2017).
10. Bird, A. W. & Hyman, A. A. Building a spindle of the correct length in human cells requires the interaction between TPX2 and Aurora A. *J. Cell Biol.* **182**, 289–300 (2008).
11. Joukov, V., De Nicolo, A., Rodriguez, A., Walter, J. C. & Livingston, D. M. Centrosomal protein of 192 kDa (Cep192) promotes centrosome-driven spindle assembly by engaging in organelle-specific Aurora A activation. *Proc. Natl. Acad. Sci. U. S. A.* **107**, 21022–7 (2010).

12. Kufer, T. A. *et al.* Human TPX2 is required for targeting Aurora-A kinase to the spindle. *J. Cell Biol.* **158**, 617–23 (2002).
13. Nikonova, A. S. *et al.* Aurora A kinase (AURKA) in normal and pathological cell division. *Cell. Mol. Life Sci.* **70**, 661–87 (2013).
14. Burgess, S. G. *et al.* Mitotic spindle association of TACC3 requires Aurora-A-dependent stabilization of a cryptic α-helix. *EMBO J.* **37**, (2018).
15. Levinson, N. M. The multifaceted allosteric regulation of Aurora kinase A. *Biochemical Journal* **475**, 2025–2042 (2018).
16. Dodson, C. A. & Bayliss, R. Activation of Aurora-A Kinase by Protein Partner Binding and Phosphorylation Are Independent and Synergistic. *J. Biol. Chem.* **287**, 1150–1157 (2012).
17. Zorba, A. *et al.* Molecular mechanism of Aurora A kinase autophosphorylation and its allosteric activation by TPX2. *Elife* **3**, (2014).
18. Floyd, S., Pines, J. & Lindon, C. APC/CCdh1 Targets Aurora Kinase to Control Reorganization of the Mitotic Spindle at Anaphase. *Curr. Biol.* **18**, 1649–1658 (2008).
19. Honda, K. *et al.* Degradation of human Aurora2 protein kinase by the anaphase-promoting complex-ubiquitin-proteasome pathway. *Oncogene* **19**, 2812–2819 (2000).
20. Bertolin, G. *et al.* Aurora kinase A localises to mitochondria to control organelle dynamics and energy production. *Elife* **7**, (2018).
21. Büchel, G. *et al.* Association with Aurora-A Controls N-MYC-Dependent Promoter Escape and Pause Release of RNA Polymerase II during the Cell Cycle. *Cell Rep.* **21**, 3483–3497 (2017).
22. Byrum, A. K. *et al.* Mitotic regulators TPX2 and Aurora A protect DNA forks during replication stress by counteracting 53BP1 function. *J. Cell Biol.* **218**, 422–432 (2019).
23. Plotnikova, O. V. *et al.* Calmodulin activation of Aurora-A kinase (AURKA) is required during ciliary disassembly and in mitosis. *Mol. Biol. Cell* **23**, 2658–2670 (2012).
24. Abdelbaki, A. *et al.* AURKA destruction is decoupled from its activity at mitotic exit but essential to suppress interphase activity. *J. Cell Sci.* **133**, jcs.243071 (2020).
25. Zhu, F. *et al.* The Mammalian SPD-2 Ortholog Cep192 Regulates Centrosome Biogenesis. *Curr. Biol.* **18**, 136–141 (2008).
26. Edelstein, A. D. *et al.* Advanced methods of microscope control using μManager software. *J. Biol. Methods* **1**, 10 (2014).
27. Schindelin, J. *et al.* Fiji: An open-source platform for biological-image analysis. *Nature Methods* **9**, 676–682 (2012).
28. Peng, J.-Y. *et al.* Automatic Morphological Subtyping Reveals New Roles of Caspases in Mitochondrial Dynamics. *PLoS Comput. Biol.* **7**, e1002212 (2011).
29. Grant, R. *et al.* Constitutive regulation of mitochondrial morphology by Aurora A kinase depends on a predicted cryptic targeting sequence at the N-terminus. *Open Biol.* **8**, 170272 (2018).
30. Buckley, D. L. *et al.* Targeting the von Hippel–Lindau E3 Ubiquitin Ligase Using Small Molecules To Disrupt the VHL/HIF-1α Interaction. *J. Am. Chem. Soc.* **134**, 4465–4468 (2012).
31. Lu, J. *et al.* Hijacking the E3 Ubiquitin Ligase Cereblon to Efficiently Target BRD4. *Chem. Biol.* **22**, 755–763 (2015).
32. Zoppi, V. *et al.* Iterative Design and Optimization of Initially Inactive Proteolysis Targeting Chimeras (PROTACs) Identify VZ185 as a Potent, Fast, and Selective von Hippel-Lindau (VHL) Based Dual Degrader Probe of BRD9 and BRD7. *J. Med. Chem.* **62**, 699–726 (2019).
33. Lindon, C., Grant, R. & Min, M. Ubiquitin-Mediated Degradation of Aurora Kinases. *Front. Oncol.* **5**, 307 (2015).
34. Sackton, K. L. *et al.* Synergistic blockade of mitotic exit by two chemical inhibitors of the APC/C. *Nature* **514**, 646–649 (2014).
35. Courtheoux, T. *et al.* Aurora A kinase activity is required to maintain an active spindle assembly checkpoint during prometaphase. *Journal of Cell Science* **131**, (2018).
36. Wysong, D. R., Chakravarty, A., Hoar, K. & Ecsedy, J. A. The inhibition of Aurora A abrogates the mitotic delay induced by microtubule perturbing agents. *Cell Cycle* **8**, 876–888 (2009).
37. Yu, F. *et al.* Aurora-A promotes the establishment of spindle assembly checkpoint by priming the Haspin-Aurora-B feedback loop in late G2 phase. *Cell Discov.* **3**, 16049 (2017).
38. Brito, D. A. & Rieder, C. L. Mitotic Checkpoint Slippage in Humans Occurs via Cyclin B Destruction in the Presence of an Active Checkpoint. *Curr. Biol.* **16**, 1194–1200 (2006).
39. Collin, P., Nashchekina, O., Walker, R. & Pines, J. The spindle assembly checkpoint works like a rheostat rather than a toggle switch. *Nat. Cell Biol.* **15**, 1378–1385 (2013).
40. Littlepage, L. E. & Ruderman, J. V. Identification of a new APC/C recognition domain, the A box, which is required for the Cdh1-dependent destruction of the kinase Aurora-A during mitotic exit. *Genes Dev.* **16**, 2274–85 (2002).

41. Crane, R. *et al.* Requirements for the destruction of human Aurora-A. *J. Cell Sci.* **117**, 5975–83 (2004).
42. Kitajima, S. *et al.* Constitutive phosphorylation of aurora-a on ser51 induces its stabilization and consequent overexpression in cancer. *PLoS One* **2**, e944 (2007).
43. Floyd, S. *et al.* Spatiotemporal organization of Aurora-B by APC/CCdh1 after mitosis coordinates cell spreading through FHOD1. *J. Cell Sci.* **126**, 2845–2856 (2013).
44. Salami, J. *et al.* Androgen receptor degradation by the proteolysis-targeting chimera ARCC-4 outperforms enzalutamide in cellular models of prostate cancer drug resistance. *Commun. Biol.* **1**, 100 (2018).
45. Smith, B. E. *et al.* Differential PROTAC substrate specificity dictated by orientation of recruited E3 ligase. *Nat. Commun.* **10**, 131 (2019).
46. Bondeson, D. P. *et al.* Lessons in PROTAC Design from Selective Degradation with a Promiscuous Warhead. *Cell Chem. Biol.* **25**, 78-87.e5 (2018).
47. Joukov, V., Walter, J. C. & De Nicolo, A. The Cep192-Organized Aurora A-Plk1 Cascade Is Essential for Centrosome Cycle and Bipolar Spindle Assembly. *Mol. Cell* **55**, 578–591 (2014).
48. Lebraud, H., Wright, D. J., Johnson, C. N. & Heightman, T. D. Protein Degradation by In-Cell Self-Assembly of Proteolysis Targeting Chimeras. *ACS Cent. Sci.* **2**, 927–934 (2016).
49. Gallini, S. *et al.* NuMA phosphorylation by aurora-a orchestrates spindle orientation. *Curr. Biol.* **26**, 458–469 (2016).
50. Lake, E. W. *et al.* Quantitative conformational profiling of kinase inhibitors reveals origins of selectivity for Aurora kinase activation states. *Proc. Natl. Acad. Sci. U. S. A.* **115**, E11894–E11903 (2018).
51. Bibby, R. A. *et al.* A cancer-associated Aurora a mutant is mislocalized and misregulated due to loss of interaction with TPX2. *J. Biol. Chem.* **284**, 33177–33184 (2009).
52. Grant, R. *et al.* Constitutive regulation of mitochondrial morphology by Aurora A kinase depends on a predicted cryptic targeting sequence at the N-terminus. *Open Biol.* (2018). doi:10.1098/rsob.170272
53. Chamberlain, P. P. & Hamann, L. G. Development of targeted protein degradation therapeutics. *Nature Chemical Biology* **15**, 937–944 (2019).
54. Lu, Y., Wang, W. & Kirschner, M. W. Specificity of the anaphase-promoting complex: A single-molecule study. *Science (80-.).* **348**, 1248737 (2015).
55. Kim, K. *et al.* Disordered region of cereblon is required for efficient degradation by proteolysis-targeting chimera. *Sci. Rep.* **9**, 1–14 (2019).
56. Bai, M. *et al.* Two newly identified sites in the N-terminal regulatory domain of Aurora-A are essential for auto-inhibition. *Biotechnol. Lett.* **36**, 1595–1604 (2014).
57. Bayliss, R., Sardon, T., Vernos, I. & Conti, E. Structural Basis of Aurora-A Activation by TPX2 at the Mitotic Spindle. *Mol. Cell* **12**, 851–862 (2003).
58. Ruff, E. F. *et al.* A dynamic mechanism for allosteric activation of Aurora kinase A by activation loop phosphorylation. *Elife* **7**, (2018).

Table 1: Summary of PROTAC compounds tested

Cpd	Substrate ligand ('warhead')	E3 ligand target	linker length (Mr)
A	MLN8237 (alisertib)	VHL	288
B	MLN8237	CRBN	272
C	MLN8237	VHL	200
D	MLN8237	CRBN	316
DX	MLN8237	CRBN	404
E	MLN8237	VHL	244
F	MLN8237	CRBN	228
G	MLN8237	VHL	156
H	MLN8237	CRBN	184

Figure 1

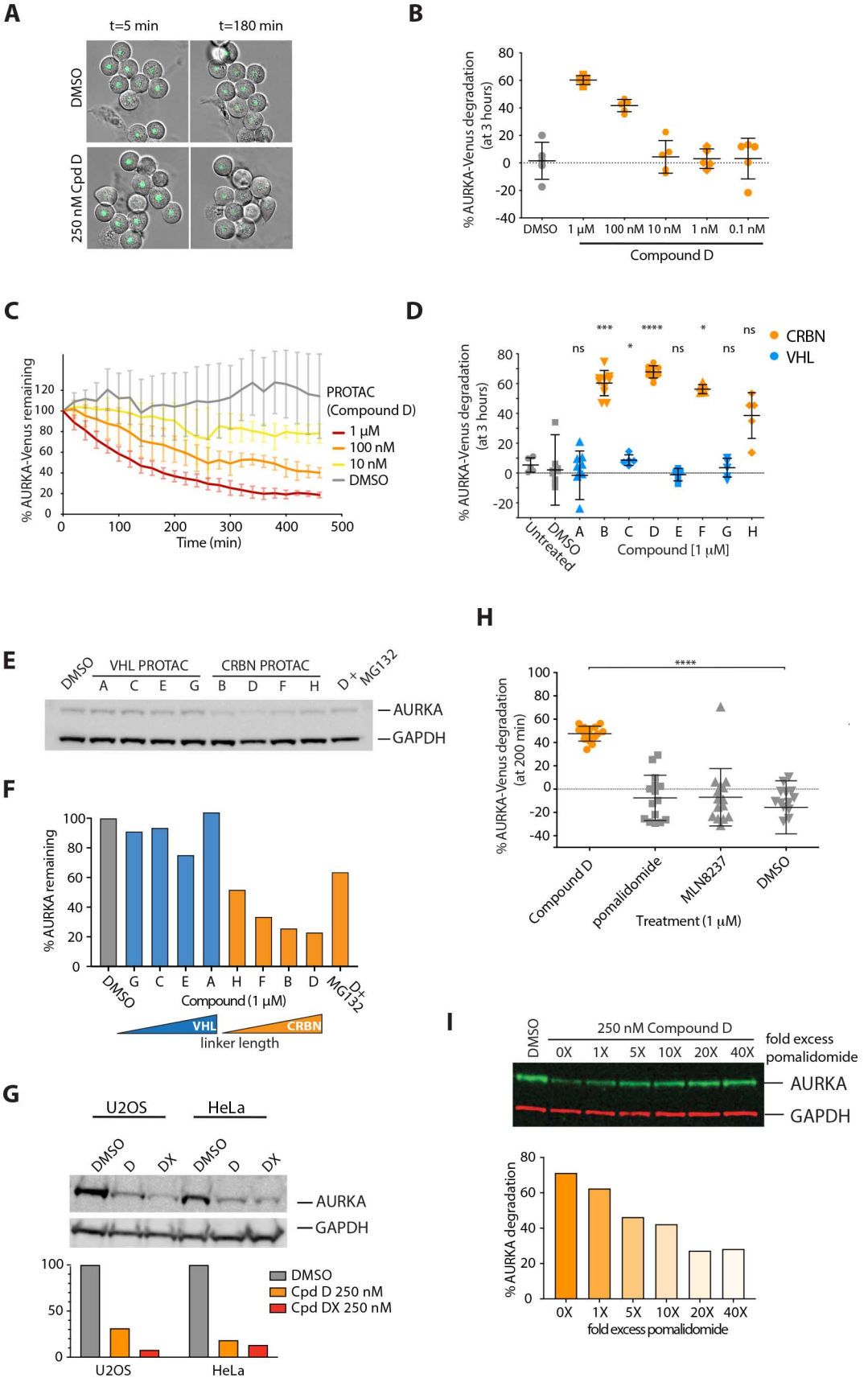
A
t=5 min
t=180 min
DMSO
250 nM Cpd D
B
% AURKA-Venus degradation (at 3 hours)
DMSO
1 μM
100 nM
10 nM
1 nM
0.1 nM
Compound D
C
% AURKA-Venus remaining
PROTAC (Compound D)
1 μM
100 nM
10 nM
DMSO
Time (min)
D
% AURKA-Venus degradation (at 3 hours)
CRBN
VHL
Untreated
DMSO
Compound [1 μM]
E
DMSO
VHL PROTAC
CRBN PROTAC
D+MG132
AURKA
GAPDH
F
% AURKA remaining
Compound (1 μM)
VHL
CRBN
linker length
G
U2OS
HeLa
DMSO
D
DX
AURKA
GAPDH
Cpd D 250 nM
Cpd DX 250 nM
H
% AURKA-Venus degradation (at 200 min)
Compound D
pomalidomide
MLN8237
DMSO
Treatment (1 μM)
I
250 nM Compound D
fold excess pomalidomide
0X
1X
5X
10X
20X
40X
AURKA
GAPDH
% AURKA degradation
fold excess pomalidomide

Figure 1 AURKA destruction following treatment with CUL4-based PROTACs

A-D AURKA-Venus^{KI} degradation in STLC-arrested RPE-1 cells, measured by quantitative timelapse imaging. **A** Examples of fields of cells treated with a PROTAC (Compound D) or vehicle control (DMSO). Venus fluorescence was measured in individual cells and plotted as an end-point assay (percentage of AURKA-Venus^{KI} degradation after 3 hr) (**B**) or as percentage of AURKA-Venus^{KI} remaining over time (to show the kinetics of degradation) (**C**). **B** Scatter plots showing response to different doses of PROTAC (Compound D) or DMSO, with whiskers indicating mean ± SDs. **C** Time-course of AURKA-Venus^{KI} degradation plotted as mean fluorescence ± SDs at each time point (n ≥ 7 cells). **D** Comparison of percentage degradation of AURKA-Venus^{KI} after treatment with potential PROTAC compounds directed to CUL4A (via CRBN) or CUL2 (VHL) ubiquitin ligases (listed in Table 1). Scatter plots show pooled results from two separate experimental repeats with whiskers indicating mean values and SDs. Results of Kruskal-Wallis multiple ANOVA, and the Dunn's post-hoc multiple comparison test to DMSO are indicated: ****, $p \leq 0.0001$; ***, $p \leq 0.001$; **, $p \leq 0.01$; *, $p \leq 0.05$; ns, not significant. **E-F** Degradation of endogenous AURKA in HeLa cells following 3 hr treatment with PROTACs, with or without 42 μM proteasome inhibitor MG132, measured by quantitative immunoblotting (**E**) to plot percentage protein remaining, ordered to show increasing linker size across the series (**F**). **G** U2OS and HeLa cells were treated for 3 hours with 250 nM Compound D (PROTAC-D) or a new compound with increased linker length (PROTAC-DX). Endogenous AURKA levels were measured by immunoblot and plotted as percentage remaining compared to DMSO treatment after normalization to GAPDH loading control. The experiment shown is one of two repeats that gave identical results. **H** Degradation of AURKA-Venus^{KI} was measured in prometaphase cells treated with 1 μM PROTAC-D, MLN8237 or Pomalidomide. Kruskal-Wallis multiple ANOVA, and the Dunn's post-hoc multiple comparison test to DMSO, showed that only PROTAC-D caused significant AURKA-Venus degradation; ****, $p \leq 0.0001$. **I** Degradation of endogenous AURKA was quantified by immunoblot from mitotic-enriched U2OS cells treated with 250 nM PROTAC D in the presence of 1 – 40-fold molar excess of Pomalidomide. Data representative of two experiments (the other in HeLa cells).

Only cells that did not exit mitosis during filming (scored as onset of cortical contractility followed by respreading) were included in the analyses shown in Figure 1A-D, H).

Figure 2

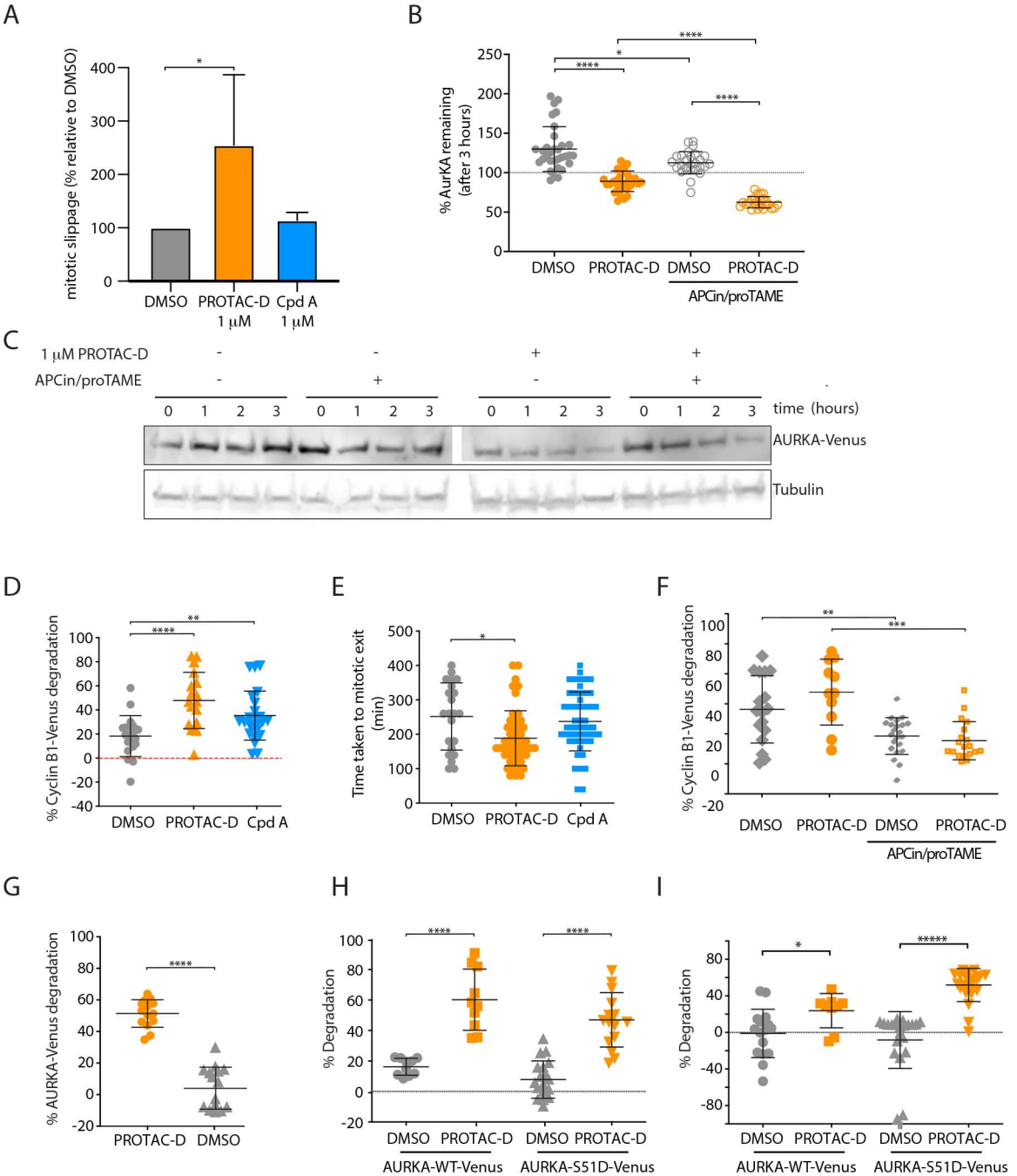
A
mitotic slippage (% relative to DMSO)
400
300
200
100
0
*
DMSO
PROTAC-D 1 μM
Cpd A 1 μM
B
% AurKA remaining (after 3 hours)
250
200
150
100
50
0
****
*
****
****
DMSO
PROTAC-D
DMSO
PROTAC-D
APCin/proTAME
C
1 μM PROTAC-D - - + +
APCin/proTAME - + - +
0 1 2 3 0 1 2 3 0 1 2 3 0 1 2 3 time (hours)
AURKA-Venus
Tubulin
D
% Cyclin B1-Venus degradation
100
80
60
40
20
0
-20
-40
**
****
DMSO
PROTAC-D
Cpd A
E
Time taken to mitotic exit (min)
500
400
300
200
100
0
*
DMSO
PROTAC-D
Cpd A
F
% Cyclin B1-Venus degradation
100
80
60
40
20
0
-20
**
***
DMSO
PROTAC-D
DMSO
PROTAC-D
APCin/proTAME
G
% AURKA-Venus degradation
100
80
60
40
20
0
-20
****
PROTAC-D
DMSO
H
% Degradation
100
80
60
40
20
0
-20
****
****
DMSO
PROTAC-D
DMSO
PROTAC-D
AURKA-WT-Venus
AURKA-S51D-Venus
I
% Degradation
80
40
0
-40
-80
*
*****
DMSO
PROTAC-D
DMSO
PROTAC-D
AURKA-WT-Venus
AURKA-S51D-Venus

Figure 2 CUL4-mediated AURKA destruction is independent of known pathways of AURKA degradation

A RPE1-AURKA-Venus^{KI} cells treated as in Figure 1D scored for mitotic slippage (exit from mitosis in presence of STLC). Percentage of cells undergoing slippage after 3 hr treatment with PROTAC-D or Cpd A is shown relative to DMSO-treated cells, mean values were generated from 3 identical experiments (where n ≥ 30 cells) and are plotted with error bars to indicate SDs and ordinary one-way ANOVA with Dunnett's post-hoc test for significance. **B-C** Degradation of AURKA-Venus in mitotic arrested RPE1-AURKAVenus^{KI} cells after treatment with PROTAC-D in the presence of APCin/proTAME, measured in single cell degradation assays (Unpaired Student's *t*-test and Mann Whitney U test for significance) (**B**) or visualised as a time-course of drug treatment by immunoblot (**C**). **D-F** RPE1-Cyclin B1-Venus^{KI} cells treated with PROTACs to investigate mitotic slippage. Increased degradation of Cyclin B1–Venus following PROTAC-D treatment (**D**), correlates with increased rate of mitotic exit (**E**) (both results statistically tested by ordinary one-way ANOVA with Dunnett's post-hoc test for significance) and is blocked by co-treatment with APC/C inhibitors APCin (40 μM) and proTAME (20 μM) (Mann Whitney U test and Unpaired Student's *t*-test for significance) (**F**). **G-I** 'Non-degradable' AURKA-Venus is degraded efficiently in response to PROTAC-D: AURKA-Venus-Δ32-66 (ΔA-box) expressed in RPE1 cells (tet-inducible RPE1-FRT/TO pool) is sensitive to PROTAC-D (Unpaired Student's *t*-test for significance) (**G**). WT or Ser51D versions of AURKA-Venus transiently electroporated into U2OS cells are equally sensitive to PROTAC-D treatment in either mitotic cells arrested by STLC (**H**) or interphase cells (**I**) (Mann Whitney U test and Unpaired Student's *t*-test for significance). Ongoing protein synthesis is likely to mask the degradation rate of Venus-tagged protein in interphase cells.

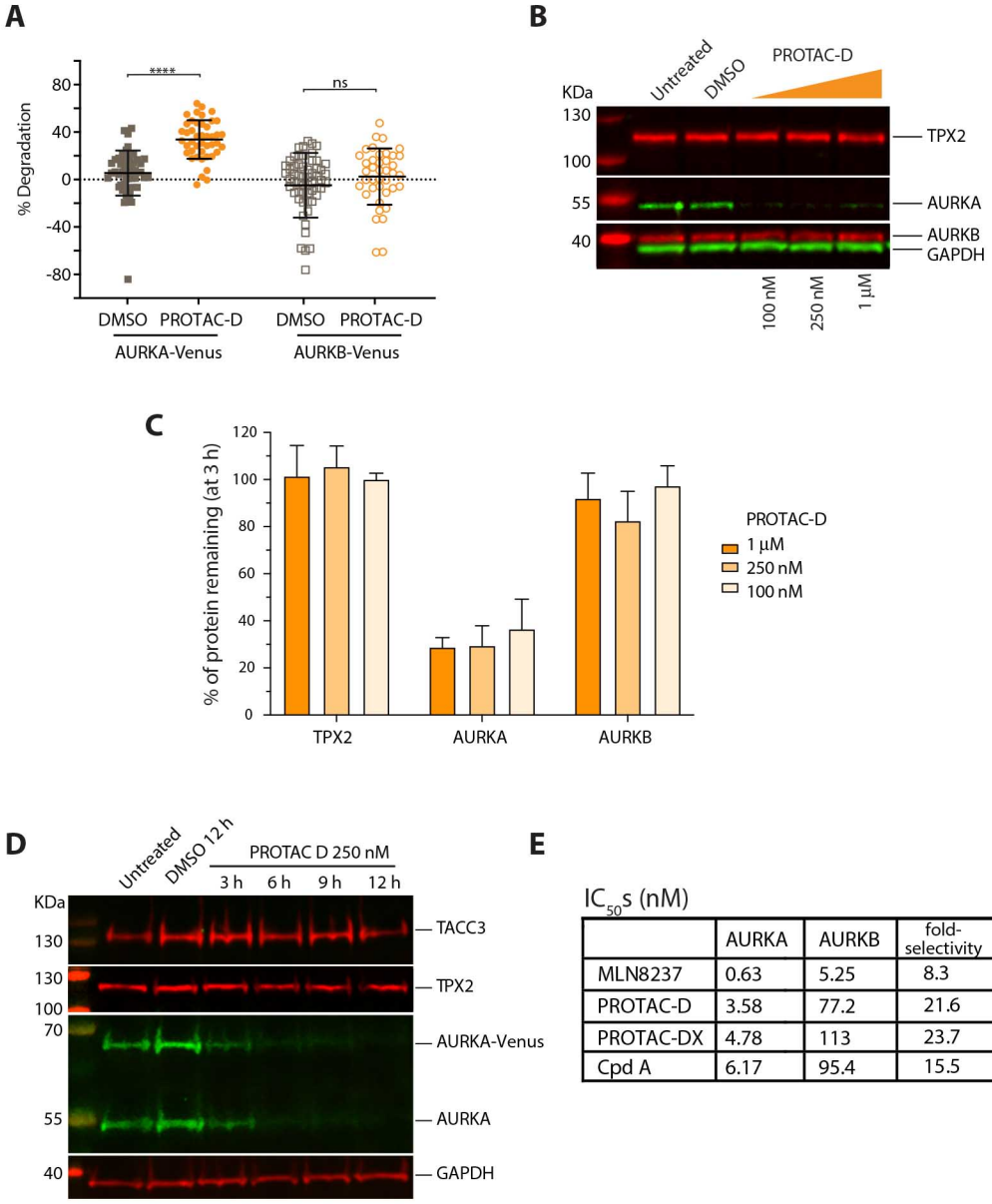

	AURKA	AURKB	fold-selectivity
MLN8237	0.63	5.25	8.3
PROTAC-D	3.58	77.2	21.6
PROTAC-DX	4.78	113	23.7
Cpd A	6.17	95.4	15.5

Figure 3 Specificity of AURKA targeting by PROTAC-D

A U2OS cells expressing tet-inducible AURKA-Venus and AURKB-Venus were arrested in mitosis with STLC and treated with 250 nM PROTAC-D for 3 hr. Scatter plot with mean values and SDs indicated show percentage degradation of protein in individual cells pooled from three separate experiments (Mann Whitney U test for significance). **B-D** Endogenous levels of AURKA interactors TPX2 and TACC3, or of AURKB, were examined by quantitative immunoblotting of extracts from cells arrested in mitosis with STLC and treated with PROTAC-D or vehicle control (DMSO). **B** HeLa cells treated for 3 hours, immunoblot representative of data from three identical experiments quantified and presented in **C** as bar charts showing mean percentages of protein remaining after PROTAC-D treatment, relative to DMSO treatment, with error bars to indicate SDs. **D** RPE1 AURKA-Venus^{KI} cells treated for 12 hours, immunoblot from one experiment. **E** Kinetics of inhibition (IC_{50}) in *in vitro* kinase assays confirms selectivity of PROTAC-D and PROTAC-DX for AURKA over AURKB: Compounds were tested in AURKA or AURKB Z-lyte CR kinase assays (Thermofisher Scientific) using [ATP] of 10 μM (AURKA) or 75 μM (AURKB), according to the K_m of the kinase. Results are shown as geometric means of three repeats (MLN8237, PROTAC-D, -DX) or two (Cpd A).

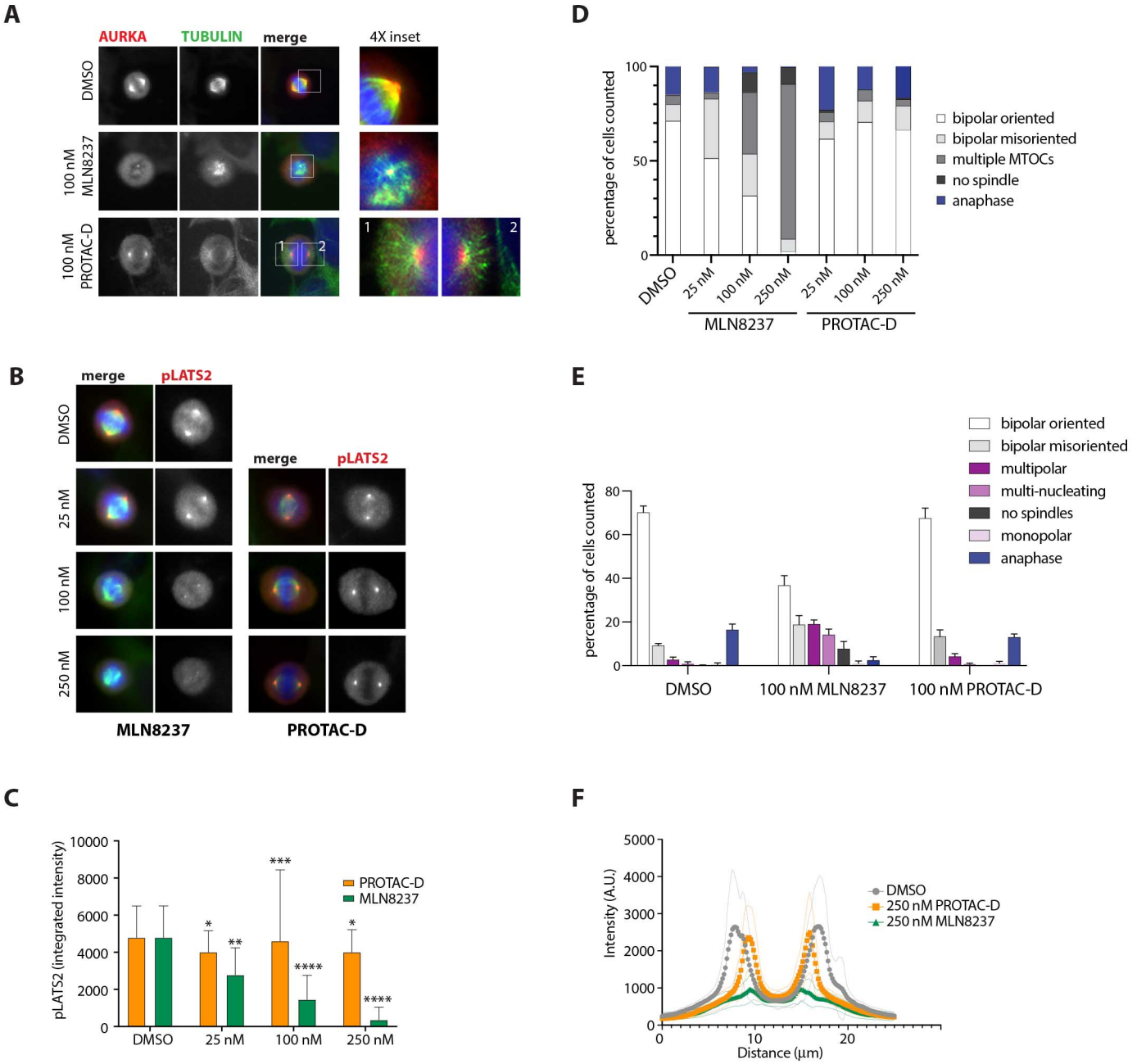

Figure 4 AURKA remains active at centrosomes upon PROTAC treatment

A-C Immunofluorescence analyses of U2OS cells synchronized through mitosis and treated for 3 hours with MLN8237, PROTAC-D or DMSO vehicle control. MLN8237 is inhibitory to MT nucleation throughout the mitotic cell. AURKA staining is retained at the centrosomes after PROTAC-D treatment (**A**) whilst a marker for active AURKA at centrosomes, p(Ser83)LATS2, persists after PROTAC-D treatment but not MLN8237 treatment (**B,C**). **C** Measurement of centrosomal pLATS2 staining from immunofluorescence images after cytoplasmic background subtraction (Kruskal-Wallis multiple ANOVA, and the Dunn's post-hoc multiple comparison test to DMSO for significance). **D,E** Mitotic phenotypes scored from TPX2/DAPI staining of fixed cells (categories illustrated in Supplementary Figure S1). **D** Dose-dependence of phenotypes using pooled data from 3 coverslips for each condition from a single experiment. **E** Mitotic categories scored at a single dose (100 nM), using data from 2 coverslips each from 3 independent repeats of the experiment, mean values ± SDs for each experiment are plotted. **F** Line-scans through fixed mitotic cells stained with pLATS2 (as shown in Figure 4B), to show both poles of the spindle (visible as maxima of staining intensity), reveal reduced pole-pole distance after PROTAC-D treatment. Traces show mean values from n ≥ 22 individual mitotic spindles, with fainter traces above and below representing SDs.

Figure 5

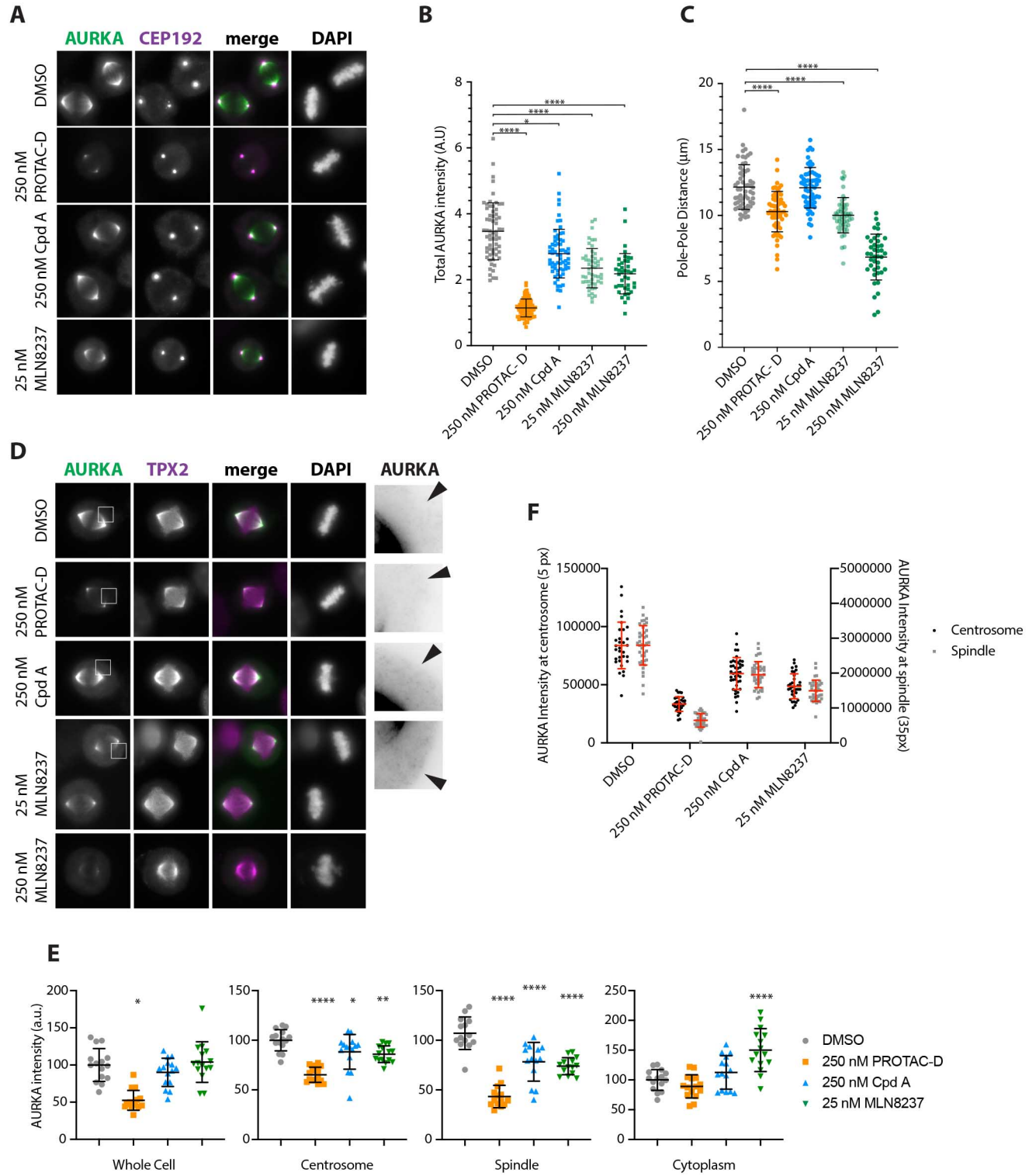
A
AURKA
CEP192
merge
DAPI
DMSO
250 nM PROTAC-D
250 nM Cpd A
25 nM MLN8237
B
Total AURKA intensity (A.U)
DMSO
250 nM PROTAC- D
250 nM Cpd A
25 nM MLN8237
250 nM MLN8237
C
Pole-Pole Distance (µm)
D
AURKA
TPX2
merge
DAPI
E
AURKA intensity (a.u.)
Whole Cell
Centrosome
Spindle
Cytoplasm
DMSO
250 nM PROTAC-D
250 nM Cpd A
25 nM MLN8237
F
AURKA Intensity at centrosome (5 px)
AURKA Intensity at spindle (35px)
Centrosome
Spindle

Figure 5 PROTAC specifically depletes AURKA on the mitotic spindle

U2OS cells released from a single thymidine block into APCin and ProTAME to arrest at metaphase and pre-treated for 3 hours with DMSO, PROTAC-D, CpdA or MLN8237 before fixation. Cells were then stained for AURKA, CEP192, and DAPI **(A-C)**, or AURKA, TPX2 and DAPI **(D-F)**. **A** Examples of cells imaged under different drug treatments and used for measurement of total AURKA intensity after background subtraction (**B**) or measurement of spindle pole separation as distance from one CEP192-marked centrosome to the other (**C**). **B,C** Results of Kruskal-Wallis multiple ANOVA, and the Dunn's post-hoc multiple comparison test to DMSO are indicated, $n \geq 41$. Results are representative of two identical experiments. **D** Examples of cells imaged under different drug treatments and used to compare AURKA levels on the spindle and at the spindle poles. Insets indicated with white boxes in AURKA channel are enlarged 4X in righthand panels and have contrast increased to reveal cytoplasmic levels of AURKA (arrowheads). **E,F** Integrated AURKA intensities were measured within circles of fixed diameter centred on the centrosomes, spindle or cytoplasm to show the effect of PROTAC-D treatment on different pools of AURKA and reveal that loss of AURKA from spindle and centrosomes in control drug treatments is reflected in increased cytoplasmic levels (**E**) and that PROTAC-D treatment causes greater loss of AURKA from the spindle than from the centrosomes (**F**). Scatter plots with means ± SDs indicated show measurements from individual cells from a single experiment, and are representative of two identical experiments. For plot E, values are normalized to mean DMSO levels and ordinary one-way ANOVA with Dunnett's post-hoc test for significance to DMSO are indicated. For plot **F**, raw values are plotted using separate Y axes for centrosome and spindle values (integrated over circles of 5 and 35 pixel diameters, respectively). Scalebars in **A** and **D**, 10 μm.

Figure 6

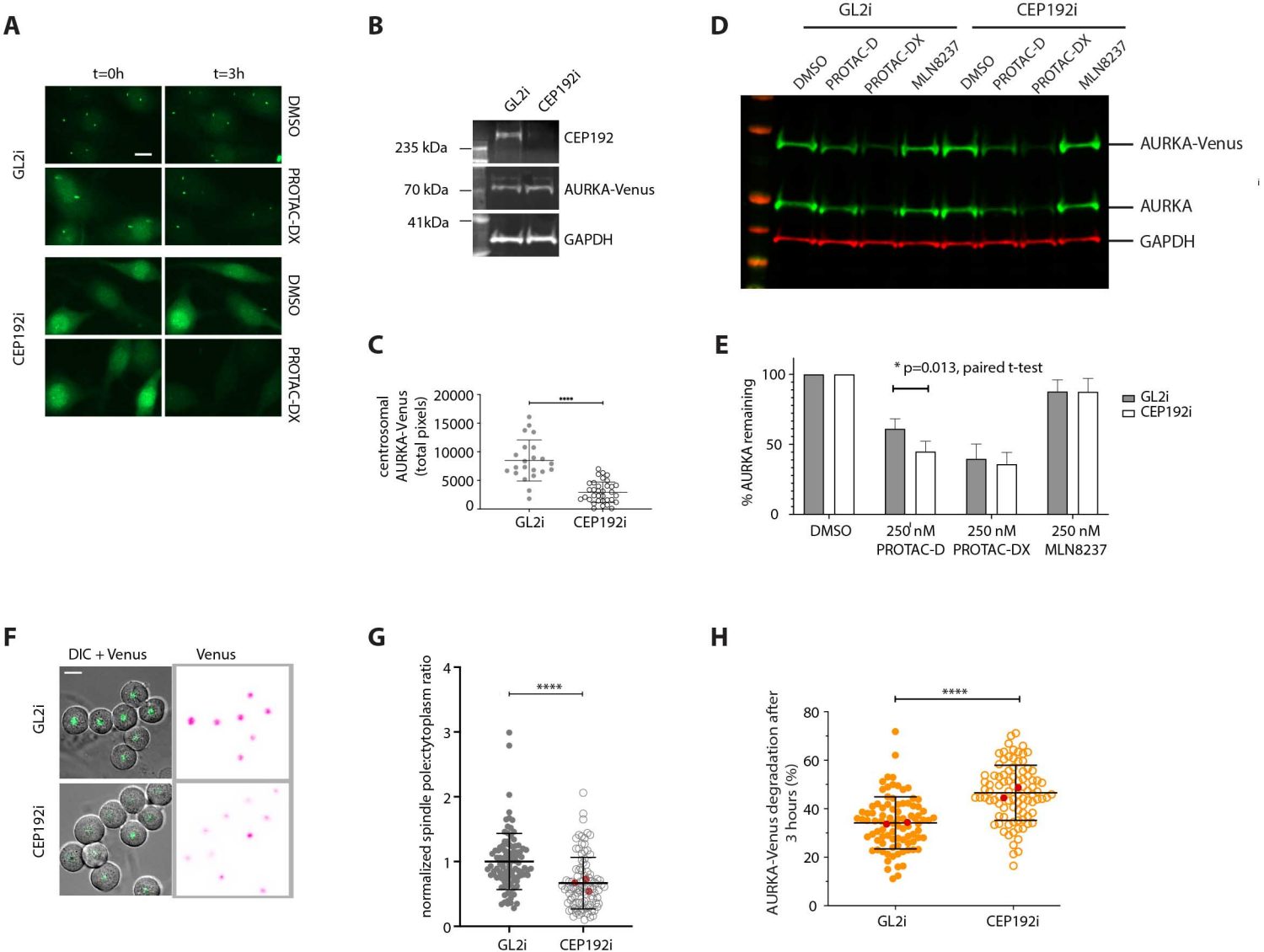
A
t=0h
t=3h
GL2i
CEP192i
DMSO
PROTAC-DX
DMSO
PROTAC-DX
B
GL2i
CEP192i
235 kDa
70 kDa
41kDa
CEP192
AURKA-Venus
GAPDH
D
GL2i
CEP192i
DMSO
PROTAC-D
PROTAC-DX
MLN8237
DMSO
PROTAC-D
PROTAC-DX
MLN8237
AURKA-Venus
AURKA
GAPDH
C
centrosomal AURKA-Venus (total pixels)
20000
15000
10000
5000
0
****
GL2i
CEP192i
E
% AURKA remaining
100
50
0
* p=0.013, paired t-test
GL2i
CEP192i
DMSO
250 nM PROTAC-D
250 nM PROTAC-DX
250 nM MLN8237
F
DIC + Venus
Venus
GL2i
CEP192i
G
normalized spindle pole:cytoplasm ratio
4
3
2
1
0
****
GL2i
CEP192i
H
AURKA-Venus degradation after 3 hours (%)
80
60
40
20
0
****
GL2i
CEP192i

Figure 6 AURKA sequestered at centrosomes is resistant to PROTAC treatment

A-E RPE1-AURKA-Venus^{KI} cells were transfected for 48 hours with siRNA against CEP192 (CEP192i) or control siRNA (GL2i) then arrested in G2 phase with RO3306 for 16 hours before treatment with PROTAC-DX for 3 hours. **A** Panels from start and end of experiment show AURKA-Venus preserved at centrosomes in control cells even following PROTAC treatment, but absent from centrosomes in CEP192i. Successful depletion of CEP192 was shown by immunoblot of cell extracts (**B**) and depletion of AURKA-Venus^{KI} from centrosomes confirmed by measurement of average pixel intensity over a fixed region of interest around each centrosome, shown as scatter plot of values from individual centrosomes with mean ± SDs indicated, and Student's *t*-Test for significance) (**C**)**.** Immunoblot of whole cell extracts showed that depletion of AURKA in response to PROTAC-D is enhanced by CEP192i, and this effect appeared significant for endogenous AURKA (**D**,**E**) but not for AURKA-Venus (Supplementary Figure S4). **A-D** show data from a single experiment and are representative of three independent experiments whilst **E** shows mean ± SDs from quantified immunoblots of all 3 experiments (Paired *t*-Test for significance). **F-H** AURKA-Venus^{KI} cells prepared in parallel with those shown in (**A**) were arrested in mitosis with STLC (instead of RO3306). Under these conditions, AURKA shows reduced localization to the single spindle pole in each cell, as shown in panels in **F** and quantified in **G**. Mean pixel intensities of AURKA-Venus were measured within a region of interest of fixed diameter around poles and in the cytoplasm, and are expressed as the ratio of spindle pole:cytoplasm after normalization of each dataset with the mean value of the control sample (Mann Whitney U test for significance) (**G**). Data from individual cells in 3 independent repeats of the experiment were pooled, with the mean value of each repeat plotted in red. **H** In mitotic-arrested cells AURKA-Venus^{KI} showed strongly enhanced degradation after CEP192 knockdown in live cell degradation assays (Mann Whitney U test for significance). Plots in **H** show percentage degradation in individual cells after 3 hours treatment and contain pooled data from 2 independent experiments with mean values from each experiment plotted in red. The result is representative of 3 independent experiments. The third experiment, showing the same result but with response to PROTAC reduced in all conditions, is shown in Supplementary Figure S4. Scalebar in **A**, 10 μm

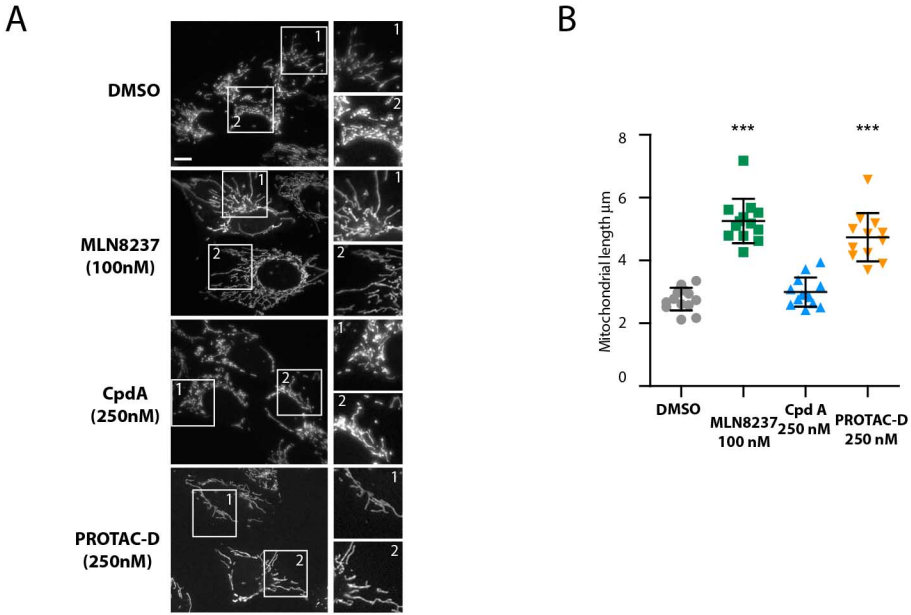

Figure 7 PROTAC-D treatment restores the mitochondrial network in FZR1^{KO} cells

U2OS FZR1^{KO} cells, in which mitochondria are highly fragmented due to the presence of excess AURKA[24], were treated for 3 hours with DMSO or with MLN8237, Cpd A or PROTAC-D at the doses indicated. Cells were then stained with Mitotracker Red^{TM}, imaged and analysed for mitochondrial fragment lengths as described in materials and methods. **A** Representative images of cells analysed. Scalebar, 10µm. **B** Scatter plots showing mean mitochondrial lengths, mean and SDs under different drug treatments. Each datapoint represents the mean value from 30 mitochondria per cell, n ≥ 12 cells. ***, p ≤ 0.001 using two-tailed Mann Whitney U test. The data are from a single experiment that is representative of two identical repeats of the same experiment.